Hyperbolic Carbon Nanoforest for Phase Matching of Ordinary and Backward Electromagnetic Waves: Second Harmonic Generation

Alexander K. Popov,*,[†] Igor S. Nefedov,[‡,§] and Sergey A. Myslivets[∥,⊥]

[†]Birck Nanotechnology Center, Purdue University, West Lafayette, Indiana 47907, United States
[‡]Aalto University, School of Electrical Engineering, P.O. Box 13000, 00076 Aalto, Finland
[§]Laboratory Nanooptomechanics, ITMO University, St. Petersburg, 197101, Russia
[∥]Kirensky Institute of Physics, Federal Research Center KSC SB RAS, 660036 Krasnoyarsk, Russia
[⊥]Siberian Federal University, 79 Svobodny pr., 660041 Krasnoyarsk, Russia

S *Supporting Information*

ABSTRACT: We show that a deliberately engineered dispersive metamaterial slab can enable the coexistence and phase matching of ordinary fundamental and contra-propagating backward second harmonic electromagnetic waves. Energy flux and phase velocity are contra-directed in the backward waves, which is the extraordinary phenomenon that gives rise to unique nonlinear optical propagation processes. We demonstrate that frequencies, phase, and group velocities, as well as the losses inherent to the guided electromagnetic modes supported by such metamaterial, can

be tailored to maximize the conversion of frequencies and to reverse the propagation direction of the generated second harmonic wave. Such a possibility, which is of paramount importance for nonlinear photonics, is proven using a numerical model describing the hyperbolic metamaterial made of carbon nanotubes standing on the metal surface. Extraordinary properties of the backward-wave second harmonic generation in the reflection direction and of the corresponding frequency doubling metareflector in the THz are investigated with a focus on the pulsed regime.

KEYWORDS: *hyperbolic metamaterials, carbon nanotubes, backward electromagnetic waves, second harmonic generation*
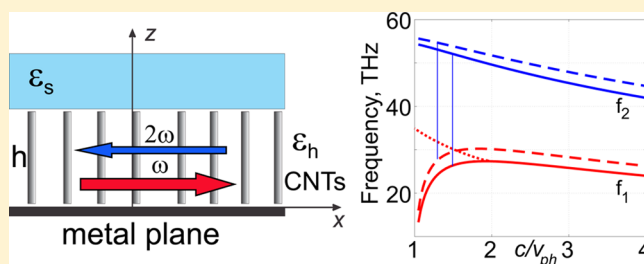
Metamaterials (MMs) can enable exotic electromagnetic waves with contra-directed phase velocity and energy flux. Such waves are commonly referred to as backward electromagnetic waves (BEMWs). In the further consideration, the waves with co- and contra-directed Poynting and wave vectors will be referred to as ordinary and extraordinary waves correspondingly. It was earlier predicted that BEMWs can pave the way to remarkable advances and extraordinary features in nonlinear optics such as greatly enhanced optical parametric amplification and frequency up- or down-shifted nonlinear reflectivity,[1] unusual features in the second harmonic generation (SHG),[1,2] and extraordinary transient processes in the three-wave mixing of ordinary and BEMWs in the pulsed regime.[3] The possibility to achieve phase matching, that is, equality of the phase velocities of the coupled ordinary and BEMWs, is the prerequisite of a fundamental importance for realizing such advances. Current mainstream in producing the BEMWs grounds on the use of the negative-index MMs (NIMs).[4] The negative-index resonance is usually narrow, and phase matching of the ordinary and BEMWs present a significant challenge.[5] The possibility of the birefringent type phase matching of ordinary EMWs in hyperbolic MMs was investigated recently in ref 6. Quasi-phase-matching of contra-propagating ordinary waves is limited to the spatially

periodically modulated nonlinear crystals. An alternative paradigm for phase matching of *backward-wave* SH and *ordinary* fundamental EMW was proposed in ref 7. The suggested approach was based on the employment of the negative spatial dispersion $\partial\omega/\partial k < 0$[8,9] and on the possibility of realizing such a dispersion in the MM made of carbon nanotubes (CNTs).[10,11] In this paper, we present the investigations that prove the possibility to fulfill a set of the above outlined requirements along with the negative dispersion in order to achieve BWSHG. The focus is on the tailored nanoengineering of the MMs, which can support opposite sign of the spatial dispersion at the fundamental and its doubled frequencies while providing for their phase matching. The indicated properties are of a paramount importance for the coherent nonlinear optics and for the related fields of photonics. The dispersion, group velocities, and losses pertinent to such modes, unusual properties, and advantages of SHG in such MMs, as well as properties of the corresponding frequency-doubling metareflector in the THz, are demonstrated through numerical simulations.

1. ELECTROMAGNETIC WAVES IN THE CARBON NANOFOREST

The underlying physical principle is based on the relationship $\mathbf{S} = \mathbf{v}_g U$ between the Poynting vector $\mathbf{S}$, group velocity $\mathbf{v}_g = \text{grad}_k \omega(\mathbf{k})$ and the energy density U. In the case of waves propagating along the axis x, it reads $\mathbf{S} = (\mathbf{S}/k)(\partial \omega / \partial k_x)$. It is seen that the energy flux $\mathbf{S}$ becomes directed against the wavevector $\mathbf{k}$ if the dispersion becomes negative: $\partial \omega / \partial k_x < 0$. To realize such the opportunity, we propose the MM model as follows. Consider finite-thickness slab of metallic CNTs of height h embedded into a host matrix with relative permittivity ϵ_h standing on a metal surface and open to the upper dielectric layer with relative permittivity ϵ_s (Figure 1). The nanotubes
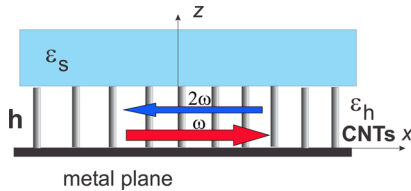
Figure 1. Geometry of free-standing CNTs.

form a two-dimensional periodic structure in the xy-plane with a square lattice (for simplicity) and a lattice constant d. Space-time dependence of the fields and the currents is taken as $\exp[-i(\omega t - k_x x)]$. Dispersion $\omega(k_x)$ of the waves propagating in the given uniaxial slab while attenuating exponentially from the interface to the upper subspace is described by equation (see Supporting Information)

$$k_z \tan(k_z h) = (\epsilon_\perp / \epsilon_s)\sqrt{k_x^2 - k^2 \epsilon_s} \tag{1}$$

where $k_z = \sqrt{\epsilon_\perp[k^2 - (k_x^2/\epsilon_{zz})]}$, k is the wavenumber in the vacuum, $k_x^2 > k^2$, $\epsilon_\perp = \epsilon_{xx} = \epsilon_{yy}$. Relative permittivity ϵ_{zz} is given by the equation[11]

$$\epsilon_{zz} = 1 - k_p^2/(k^2 + i\xi k), \quad k_p^2 = \mu_0/(d^2 L_0) \tag{2}$$

where k_p is the effective plasma wavenumber, L_0 is the effective inductance of the CNTs per unit length, the parameter $\xi = \sqrt{\epsilon_0 \mu_0}/\tau$ is responsible for losses, and τ is the electron relaxation time. Radius of the CNTs r and the lattice constant d are taken to be $r = 0.82$ nm and $d = 15$ nm. Then the indicated parameters are estimated as $L_0 = 3.7 \times 10^{-3}$ H/m, $k_p^2 = 1.51 \times 10^{12}$ m^{-2}, $\tau = 3$ ps.[11] The effective plasma frequency is calculated as $\omega_p/2\pi = 58.7$ THz. The effective medium model is employed which is valid here because a period of the lattice $d = 15$ nm is much less than the wavelengths of both fundamental and second harmonics. Thus, the MM can be thought of as a uniaxial free-electron plasma where electrons can move only along z-direction. Hence, it can be viewed as a medium with hyperbolic dispersion at frequencies below the plasma frequency $\omega_p = k_p c$ because $\epsilon_{zz} < 0$, whereas $\epsilon_\perp > 0$. Transverse polarizability of the CNTs can be neglected because electric fields do not interact with very thin CNTs. This assumption agrees with the conclusions of ref 12 for the filling factor $f < 0.07$. In our case, it is $f = 0.0094$. The same concerns the approximation $\mu \approx 1$. In our numerical simulations, we assume $\epsilon_\perp = \epsilon_s = 1$, which correspond to air.

We have calculated the complex propagation constant $k_x = k_x' + i k_x''$ by numerically solving eq 1. Dispersion diagram for two lowest modes for the two different thicknesses of the CNT

layer is shown in Figure 2. Here, reduced wave vector $k_x'/k = c/v_{ph} = n_{ph}$ is a slow-wave factor which represents effective
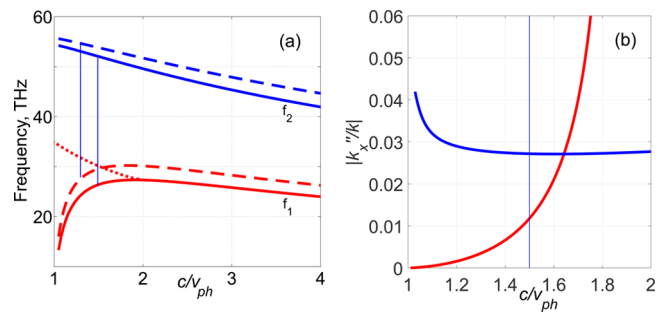
Figure 2. (a) Dispersion of two lowest eigenmodes in the slabs of standing CNTs with open ends. $\epsilon_h = \epsilon_s = 1$; $h = 1.05$ μm (the solid lines) and $h = 0.85$ μm (the dashed lines). (b) Attenuation factor k_x'' for the lower-frequency mode (the ascending red plot) and for the higher-frequency second mode (the descending blue plot) at $h = 1.05$ μm.

refraction index n_{ph}. Real part of the normalized propagation constant k_x'/k is shown for $h = 1.05$ μm (the solid lines) and $h = 0.85$ μm (the dashed lines). Vertical lines mark frequencies of the phase matched ordinary fundamental and backward SH waves. The dotted line shows real part of the normalized propagation constant for complex wave, existing in the stop band and calculated for $h = 1.05$ μm. It is seen that frequencies and dispersion of the allowed propagating EMW (eigenmodes) are determined by the height, spacing, diameter, and by the electric parameters of the nanotubes. Hence, they can be tailored. Figure 2a demonstrates the possibility of adjusting the eigenmodes so that the ordinary wave at frequency f_1 and the contra-propagating backward wave at frequency f_2 travel with the equal phase velocities. As stressed above, the latter is a requirement of a fundamental importance which gives rise to the extraordinary SHG process. A group delay factor $n_{gr} = c/v_g$ for both modes is shown in Figure 3. It is seen that at $c/v_{ph,1} = c/v_{ph,2} \approx 1.5$, which corresponds to phase matching, $n_{g,1} \approx 5.5$ and $n_{g,2} \approx 8.9$.
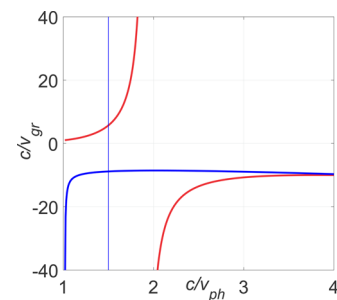
Figure 3. Group velocity vs phase velocity for the same two modes as in Figure 2 for $h = 1.05$ μm. The split red plot is for the lower-frequency mode, the ascending blue one is for the higher-frequency mode.

The dispersion displayed in Figure 2a contrasts with that in an unbounded uniaxial crystal[13]

$$k_\perp^2 = \epsilon_{zz}(k^2 - k_z^2), \quad k_\perp^2 = k_x^2 + k_y^2 \tag{3}$$

which in the given case takes the form

$$k_x^2 = [1 - k_p^2/(k^2 + ik\xi)](k^2 - k_z^2) \tag{4}$$

It also contrasts with the case of the MM made of CNTs standing between two perfectly conducting planes:

$$k_x^2 = \epsilon_{zz}[k^2 - (m\pi/2h)^2] \tag{5}$$

Here, $k_z = m\pi/(2h)$, h is the height of the waveguide, and m is a positive integer determining the number of field variations along CNTs. It is seen that in the latter case only BW propagation ($dk_x^2/dk^2 < 0$) is allowed at $\epsilon_{zz} < 0$ and $k < m\pi/2h$. The appearance of the positive dispersion for small slow-wave factors and the appearance of the stop-light regime $v_g \to 0$ in Figures 2a and 3 are explained by the fact that the Poynting vector in the upper bounding dielectric (here, air) is always codirected with the wave vector, whereas inside the metaslab they can be contra-directed. Hence, the overall energy flow inside the metaslab depends on the field variation across the metaslab. The latter depends on the relation between k_z and k_x, which is different for different eigenmodes. The dependence of the phase-matched frequencies on the nanotubes height can be used for validation of the dispersion properties.

Attenuation of EMWs along the x-axis is represented by imaginary part of the propagation constant $k_x = k_x' + ik_x''$. A magnitude of k_x'' is dependent on the electrons relaxation time in the CNTs τ at the frequencies below optical transitions. Figure 2b shows attenuation of the both modes in the proximity of the frequencies that correspond to the phase matched fundamental and BWSH waves. The branch of $f(c/v_{ph})$, which descends down to the stop light point on the dispersion curve (the red dotted line at approximately 27.5 THz for $h = 1.05$ μm), is characterized by the complex constant corresponding to a huge damping. Its imaginary part, k_z''/k, is not shown. (Such a branch is not shown for $h = 0.85$ μm either and will not be considered further.) It is seen that attenuation may become significantly different for different modes and frequencies and depends on the metaslab geometry.

2. PHASE-MATCHED BACKWARD-WAVE SECOND HARMONIC GENERATION IN THE CARBONE NANOFOREST

In the case of precise phase matching, normalized amplitudes of the fundamental harmonic (FH), a_1, and of the SH, a_2, are given by Maxwell's equations:

$$s_2(\partial a_2/\partial \xi) + (v_1/v_2)\partial a_2/\partial \tau = -igla_1^2 - (\tilde{\alpha}_2/2d)a_2 \tag{6}$$

$$s_1(\partial a_1/\partial \xi) + \partial a_1/\partial \tau = -i2g^*la_1^*a_2 - (\tilde{\alpha}_1/2d)a_1 \tag{7}$$

Here, $v_i > 0$ and $\tilde{\alpha}_{1,2} = a_{1,2}L$ are group velocities and normalized attenuation indices at corresponding frequencies; $\alpha_{1,2}$ are attenuation indices and L is the metaslab thickness. Parameters s_j take values $s_j = 1$ for the ordinary wave, and $s_j = -1$ for the backward wave. Quantities $|a_j|^2$ are proportional to the time-dependent photon fluxes: $a_j = E_j/E_{10}$, where E_j values are slowly varying amplitudes of the electric components of electromagnetic fields and E_{10} is the amplitude of the FH field at the metaslab entrance. The approximation of plane traveling waves is employed. Coupling parameter $g = \textit{æ}E_{10}$, where $\textit{æ} = \sqrt{k_1 k_2}\, 4\pi\chi_{2,\text{eff}}^{(2)}$. Here, $\chi_{2,\text{eff}}^{(2)} = \chi_{1,\text{eff}}^{(2)}/2$ are the effective nonlinear susceptibilities at the corresponding frequencies, $k_j = \omega_j/v_{ph}$, and v_{ph} is the value corresponding to phase matching. We also define normalized metaslab thickness $d = L/l$, position $\xi = x/l$ and the time instant $\tau = t/\Delta\tau$, where $l = v_1\Delta\tau$ is the

pump pulse length, and $\Delta\tau$ is the duration of the input FH pulse.

The shape of the input FH pulse was chosen to be close to the rectangular profile:

$$F(\tau) = 0.5\left(\tanh\frac{\tau_0 + 1 - \tau}{\delta\tau} - \tanh\frac{\tau_0 - \tau}{\delta\tau}\right) \tag{8}$$

Here, $\delta\tau$ presents duration of the pulse front and tail, and τ_0 is a shift of the front relative to $t = 0$. The magnitudes $\delta\tau = 0.01$ and $\tau_0 = 0.5$ were selected for numerical simulations. The following values and estimates, which are relevant to the MM made of nanotubes of height $h = 1.05$ μm (Figures 2 and 3), were also used for numerical simulations. Spectrum bandwidth corresponding to the pulse of duration $\Delta\tau = 10$ ps is on the order of $\Delta f \approx 1/\Delta\tau = 0.1$ THz. Hence, $\Delta f/f \propto 10^{-2}/10^{-3}$, and phase matching can be achieved for the whole frequency band. This becomes impossible at $\Delta\tau = 10$ fs because of $\Delta f/f \propto 10$ in this particular case. Phase matching occurs at $k_1 = 5.47 \times 10^5$ m^{-1}, $k_2 = 2k_1$ (Figure 2). Corresponding attenuation factors are calculated as $\alpha_1 = 2k_1'' = 2(9.3 \times 10^{-3})k_1 = 1.02 \times 10^4$ m^{-1}, $\alpha_2 = 2k_2'' = 2(2.72 \times 10^{-2})k_2 = 5.96 \times 10^4$ m^{-1}. Since losses for the second mode are greater, the characteristic metaslab thickness corresponding to extinction $\exp(-\alpha_2 L) = 0.1$, that is, to $\alpha_2 L = 2.4$, $\alpha_1 L = 0.41$, is estimated as $L \approx 40$ μm. The FH pulse length is estimated as $l = \Delta\tau v_1 = \Delta\tau c/n_{g,1} = 606$ μm, which is 15 times greater than L. The latter indicates that the quasistationary process establishes through almost the entire pulse duration, whereas some transients occur at the pulse forefront and tail. Note that at $\Delta\tau \leq 10$ ps, which is still acceptable, the effect of the transient processes significantly increases.

Figure 4 presents the results of numerical simulations for energy conversion efficiency at BWSHG with an account for
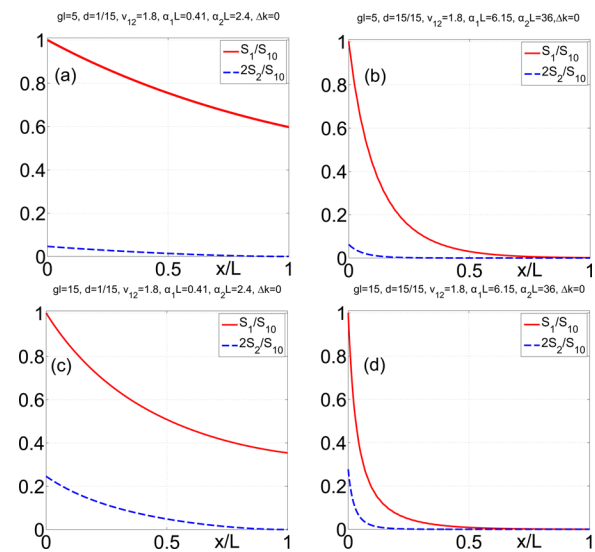
Figure 4. Backward-wave SHG: dependence of the energy conversion efficiency on the metaslab thickness, intensity, and duration of the pump pulse: (a, b) $gl = 5$; (c, d) $gl = 15$; (a, c) $L/l = 1/15$; (b, d) $L/l = 1$.

the above-calculated losses and group velocities. Here, $\eta_2(x) = S_2(x)/S_{10} = \int dt|a_2(x,t)|^2/\int dt|a_{10}(t)|^2$ is the pulse energy (quantum) conversion efficiency and the factor $S_1(x)/S_{10}$ presents depletion of energy of the FH pulse along the slab and at the corresponding exits: $x = 0$ for the SH and $x = L$ for the FH. Two coupling parameters ($gl = 5$ and $gl = 15$) and two

different input pulse lengths (L/l = 1/15, and L/l = 1) were chosen for the simulations. Coupling parameter gl is proportional to the total number of photons per input FH pulse. It can be also thoughts of as the ratio l/x_0 of the input pulse length l and the characteristic slab thickness x_0 required for the significant photon conversion from FH to SH for the given pulse intensity at its maximum. The interplay of several processes contributes to the outlined dependencies. Figure 4 shows that conversion efficiency grows with increase in the input pulse amplitude. However, the important unusual property of BWSHG, that is, frequency-doubling nonlinear reflectivity, is that it rapidly saturates with an increase of the metaslab thickness. Such unusual behavior is due to the backwardness of SH, which propagates against the FH beam and is predominantly generated in the area where both FH and SH are not yet significantly attenuated. It is seen that the overall nonlinear reflectivity provided by such a frequency-doubling meta-reflector may reach the values on the order of 10% for the selected values of the parameter gl. Calculations also show that the reflectivity in the pulse maximum for the same parameters appears 2 times greater than the time-integrated values. These dependencies are in stark contrast with SHG in ordinary materials, as seen from the comparison with Figure 5. It
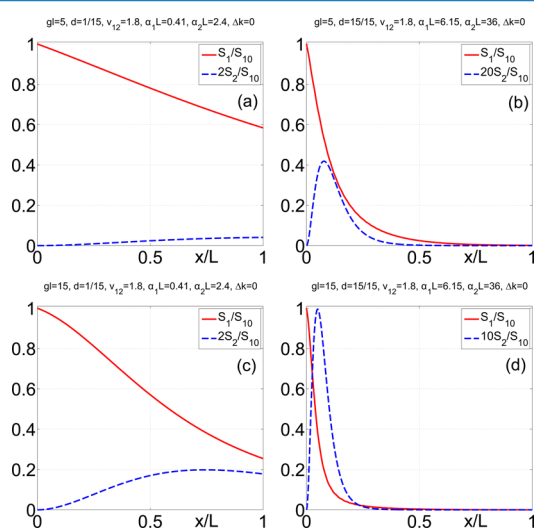
Figure 5. Ordinary SHG at all other parameters, the same as in Figure 4.

displays corresponding dependencies in the case of ordinary material with all other parameters the same as in Figure 4. Here, both FH and SH exit the slab at $x = L$. It is seen that, in general, SH reaches its maximum inside the slab. This is due to the interplay of the nonlinear conversion and the attenuation processes. In order to maximize the SH output, the pump strength, its pulse duration, and the slab thickness must be carefully optimized as shown in Figure 5c. Investigations prove that the shape and the width of the output pulses in the cases of ordinary SHG and BWSHG also appear to be significantly different.

◼ CONCLUSIONS

We show the possibility to engineer the metamaterials that satisfy to a set of requirements of a fundamental importance for the realization of extraordinary nonlinear photonic processes and devices which enable the changing of photons frequency

and propagation direction. The proposed metamaterials support a set of traveling electromagnetic waves with the properties as follows: (i) their frequencies satisfy to energy conservation law for nonlinear-optical frequency-conversion processes; (ii) some of them are extraordinary backward waves with contra-directed energy flux and phase velocity, whereas other(s) are ordinary waves; (iii) contra-propagating waves have equal phase velocities, that is, are phase matched; (iv) such properties can be adjusted to different frequencies. Frequency mixing of backward and ordinary waves possess fundamentally different properties compared to they ordinary counterparts and have important breakthrough applications in photonics. Current mainstream in crafting metamaterials that ensure backward waves relies on the engineering of mesoatoms, the nanoscopic LC circuits that provide a negative magnetic response at optical frequencies. The approach described in this paper is fundamentally different and is based on the engineering of the tailored coexisting negative and positive dispersion $\omega(k)$ of electromagnetic waves which dictates the particular relationship between the frequencies and wavevectors of normal electromagnetic modes.

Such a general possibility is demonstrated through numerical simulations making use of a particular example of the "carbon nanoforest". It is the metamaterial made of carbon nanotubes of a particular diameter, height, and spacing, standing on the metallic surface. Such metamaterial can be also viewed as a tampered waveguide. We show that the negative and sign-changing dispersions pertinent to such nanowaveguide can be tailored to support phase matched backward-wave second harmonic generation in the THz through near-IR frequency ranges. Attenuation imposed by the metallic properties of carbon nanotubes and by the guided propagation were investigated and appeared to be different for the coupled harmonics. Most practically important, pulsed, regimes of second harmonic generation in such metamaterials were investigated with the simplified model of plane traveling waves. A set of coupled partial differential equations was employed, which accounted for dispersion of group velocities and attenuations of the coupled pulses. Since the generated second harmonic travels in the direction opposite to the fundamental wave, the investigated process presents a model for the realization of a miniature frequency doubling metareflector/metaswitch with unique properties. This was demonstrated by comparison with the ordinary second harmonic generation at the otherwise similar conditions.

The described approach can be generalized to engineering the metamaterials of different architectures and composed of different materials that support the tailored positive and negative dispersion of electromagnetic waves to enable extraordinary phase-matched coherent nonlinear optical propagation processes through an extended frequency band.[14]

◼ ASSOCIATED CONTENT

⑤ Supporting Information

The Supporting Information is available free of charge on the ACS Publications website at DOI: 10.1021/acsphotonics.7b00146.

Derivation of the transfer matrix and dispersion equation (PDF).

■ AUTHOR INFORMATION

Corresponding Author
*E-mail: popov@purdue.edu.
ORCID
Alexander K. Popov: 0000-0003-4602-5708
Author Contributions
All authors contributed equally.
Notes
The authors declare no competing financial interest.

■ REFERENCES

(1) Popov, A. K.; Shalaev, V. M. Negative-index metamaterials: second-harmonic generation, Manley Rowe relations and parametric amplification. *Appl. Phys. B: Lasers Opt.* **2006**, *84*, 131−137.

(2) Shadrivov, I. V.; Zharov, A. A.; Kivshar, Y. S. Second-harmonic generation in nonlinear left-handed metamaterials. *J. Opt. Soc. Am. B* **2006**, *23*, 529−534.

(3) Slabko, V. V.; Popov, A. K.; Tkachenko, V. A.; Myslivets, S. A. Three-wave mixing of ordinary and backward electromagnetic waves: extraordinary transients in the nonlinear reflectivity and parametric amplification. *Opt. Lett.* **2016**, *41*, 3976−3979.

(4) Cai, W.; Shalaev, V. *Optical Metamaterials, Fundamentals and Applications*, 1st ed.; Springer-Verlag: New York, 2010.

(5) Lan, S.; Kang, L.; Schoen, D. T.; Rodrigues, S. P.; Cui, Y.; Brongersma, M. L.; Cai, W. Backward phase-matching for nonlinear optical generation in negative-index materials. *Nat. Mater.* **2015**, *14*, 807−811.

(6) Duncan, C.; Perret, L.; Palomba, S.; Lapine, M.; Kuhlmey, B.; de Sterke, C. M. New avenues for phase matching in nonlinear hyperbolic metamaterials. *Sci. Rep.* **2015**, *5*, 8983.

(7) Popov, A. K.; Shalaev, M. I.; Myslivets, S. A.; Slabko, V. V.; Nefedov, I. S. Enhancing coherent nonlinear-optical processes in nonmagnetic backward-wave materials. *Appl. Phys. A: Mater. Sci. Process.* **2012**, *109*, 835−840.

(8) Agranovich, V. M.; Gartstein, Y. N. Spatial dispersion and negative refraction of light. *Phys.-Usp.* **2006**, *49*, 1029. [UFN **176**, 1051−1068 (2006)].

(9) Agranovich, V. M.; Shen, Y. R.; Baughman, R. H.; Zakhidov, A. A. Linear and nonlinear wave propagation in negative refraction metamaterials. *Phys. Rev. B: Condens. Matter Mater. Phys.* **2004**, *69*, 165112.

(10) Lindell, I. V.; Tretyakov, S. A.; Nikoskinen, K. I.; Ilvonen, S. BW media - media with negative parameters, capable of supporting backward waves. *Microw Opt Technol. Lett.* **2001**, *31*, 129−133.

(11) Nefedov, I.; Tretyakov, S. Ultrabroadband electromagnetically indefinite medium formed by aligned carbon nanotubes. *Phys. Rev. B: Condens. Matter Mater. Phys.* **2011**, *84*, 113410.

(12) Krokhin, A. A.; Reyes, E.; Gumen, L. Low-frequency index of refraction for a two-dimensional metallodielectric photonic crystal. *Phys. Rev. B: Condens. Matter Mater. Phys.* **2007**, *75*, 045131.

(13) Landau, L. D.; Lifshitz, E. M. *Electrodynamics of Continuous Media*, 2nd ed.; Course of Theoretical Physics; Pergamon Press: New York, 1960; Ch. 9.

(14) Guler, U.; Zemlyanov, D.; Kim, J.; Wang, Z.; Chandrasekar, R.; Meng, X.; Stach, E.; Kildishev, A. V.; Shalaev, V. M.; Boltasseva, A. Plasmonics: Plasmonic Titanium Nitride Nanostructures via Nitridation of Nanopatterned Titanium Dioxide. *Adv. Opt. Mater.* **2017**, *5*, 1600717.